Geophysical Research Letters

RESEARCH LETTER
10.1029/2020GL090713

The Intensifying Role of High Wind Speeds on Air-Sea Carbon Dioxide Exchange

Yuanyuan Gu[1,2], Gabriel G. Katul[3,4], and Nicolas Cassar[1,5]

[1]Division of Earth and Ocean Sciences, Nicholas School of the Environment, Duke University, Durham, NC, USA, [2]College of Oceanography, Hohai University, Nanjing, China, [3]Nicholas School of the Environment, Duke University, Durham, NC, USA, [4]Department of Civil and Environmental Engineering, Duke University, Durham, NC, USA, [5]CNRS, University of Western Brittany Brest, IRD, Ifremer, LEMAR, Plouzané, France

Key Points:

- Global CO_2 fluxes at high wind speeds were estimated using a new wave-wind dependent formulation
- High wind speed events, which represent some 3% of wind conditions, contribute 18% of the global air-sea CO_2 flux
- Approximately 50% of the global flux at high wind speeds is attributed to bubbles associated with wave breaking

Supporting Information:

- Supporting Information S1

Correspondence to:

N. Cassar,
nicolas.cassar@duke.edu

Citation:

Gu, Y., Katul, G. G., & Cassar, N. (2021). The intensifying role of high wind speeds on air-sea carbon dioxide exchange. *Geophysical Research Letters*, *48*, e2020GL090713. https://doi.org/10.1029/2020GL090713

Received 8 SEP 2020
Accepted 10 FEB 2021

Abstract While it has been known that wave breaking and bubble generation at high wind speeds enhance air-sea carbon dioxide (CO_2) exchange rates (F), quantification of their contribution at the global scale remains a formidable challenge. There is urgency to make progress on this issue as a significant uptick in both magnitude and frequency of high wind events (HW) has been documented over the last 3 decades. Using a wind-wave dependent expression for gas transfer velocity (k) that explicitly considers bubbles and a widely used wind-only parameterization, the spatial pattern of k at high winds can be explained by sea surface temperature distribution. The HW, which represent some 3% of wind conditions, contribute disproportionally to the global F (18%) with an increasing trend. Approximately 50% of the global F at high winds is attributed to bubble contribution. The findings are of significance to quantifying CO_2 transfer to the ocean interior.

Plain Language Summary Studies on air-sea carbon dioxide (CO_2) exchange seek to determine how rapidly CO_2 molecules traverse the air-water interface. This exchange impacts a plethora of processes related to ocean biogeochemistry, oceanic carbon cycling, and CO_2 buildup in the atmosphere. At high wind speeds, both conventional aerodynamic transfer processes and bubbles generated by wave breaking are expected to enhance air-sea CO_2 gas exchange. Yet, the impact of bubbles in isolation on global and regional CO_2 exchange remains a subject of inquiry and speculation. There is some urgency to make progress on this topic because the magnitude and frequency of high wind events (HW) have been steadily increasing over the last 3 decades. The work here demonstrates that bubbles contribute as much as 50% of CO_2 gas exchange under high wind speeds conditions, which rarely occur over the ocean (less than 3% of the time). Yet, HW contribute disproportionally to the global air-sea CO_2 gas exchange (about 18%).

1. Introduction

Air-sea flux of carbon dioxide (CO_2; [F]) is necessary to any global carbon cycle assessment and its concomitant role in regulating the climate system. Generally, F is estimated from a water-side bulk transfer relation given as

$$F = (k)(K_0)(\Delta pCO_2) = (k)(K_0)(pCO_{2w} - pCO_{2a}) \quad (1)$$

where positive fluxes denote oceanic outgassing and negative fluxes denote uptake, K_0 is the solubility of CO_2 (mol L^{-1} atm^{-1}) assumed to vary with sea surface temperature (SST) and salinity, pCO_{2w} and pCO_{2a} are the partial pressure of CO_2 in water and air (μatm), respectively, and k is the gas transfer velocity (cm hr^{-1}) and is the subject of this letter. The parameterization of k in the open ocean has long been a challenge contributing substantial uncertainties to global estimates of F. A number of small-scale physical processes such as waves, turbulence, tidal currents, rain, subskin-to-skin temperature gradients, and surface films are known to impact k and the air-sea CO_2 exchange (Broecker et al., 1978; Frew et al., 2004; Ho et al., 1997; Watson et al., 2020; Zappa et al., 2007). However, accommodating all these physical processes and aggregating their effects at scales relevant to climate models remains a challenge. For this reason, common formulations empirically relate k to the dominant mechanism, which is the mean wind speed (U) at some reference height, usually set at 10 m. By mean U, we are referring to time-scales that are sufficiently long to average

over many water-side eddy turnover times making contact with air-water interface but short enough to resolve some aspects of the diurnal wind patterns (usually few hours). These formulations take the form of $k \propto U^n$ with $n = 1$ (Liss & Merlivat, 1986), $n = 2$ (Sweeney et al., 2007; Wanninkhof, 1992, 2014), and $n = 3$ (McGillis et al., 2001; Prytherch et al., 2010; Wanninkhof & McGillis, 1999) or similar polynomial expressions (Nightingale et al., 2000; A. Weiss et al., 2007) all being proposed and receiving partial experimental support. However, recent measurements suggest that such wind-only relations cannot be extrapolated to high U where bubble formation is likely to occur (Bell et al., 2017; Blomquist et al., 2017). At intermediate to high U, bubbles generated at the ocean surface, primarily associated with air entrainment by breaking waves, disproportionately enhance k and subsequently F (Johnson & Liss, 2014; Woolf, 1993, 1997). Significant contribution of bubbles to global k and F for CO_2 are now estimated at about 30% and 40%, respectively (Reichl & Deike, 2020; Woolf, 1997). Regionally, hurricanes predominantly occurring in tropical and subtropical oceans have been observed to significantly facilitate CO_2 exchange due to their enhanced k associated with high U (Bates, 2007; Bates et al., 1998; Huang & Imberger, 2010).

Global U above oceans have experienced an uptick in magnitude over recent decades (Young & Ribal, 2019; Young et al., 2011; Zheng et al., 2016), but tracking how this increase in U influences F via enhanced bubble formation at such large scales remains difficult (Le Quéré et al., 2010; Wanninkhof & Trinanes, 2017) thereby motivating the present work. A number of theoretical developments and data products are now offering new tools to address this question. More than 30 years of high-resolution satellite U data is enabling the detection of long-term trends associated with high winds to be unpacked and utilized in the estimation of k. High wind events (HW) predominantly occur in the midlatitudes' winters over the North Atlantic, the North Pacific, and the Subantarctic oceans. HW are generally caused by synoptic-scale transient eddies along the midlatitude strong storm track or air-sea interaction over sharp SST fronts (Chelton et al., 2004; Minobe et al., 2008; Sampe & Xie, 2007; Small et al., 2008; Spall, 2007; Xie, 2004). Over tropical oceans, HW occur infrequently (1%) and are predominantly associated with sporadic tropical cyclones (Sampe & Xie, 2007). While the impact of such extreme wind events ($U > 33$ m s^{-1}) on k has been explored in earlier studies (see references above and Lévy et al., 2012; Liang et al., 2020), the broader implications of HW on k is unclear.

On the theoretical front, a new semi-empirical equation for k that accounts for significant wave height (H_s) and separates k into contributions of turbulence and bubbles has recently been proposed (Deike & Melville, 2018). This formulation, labeled here as k_{D18}, was shown to be in agreement with a number of gas exchange experiments at low and high U (Deike & Melville, 2018) and was recently applied to explore bubble-mediated air-sea CO_2 flux (Reichl & Deike, 2020).

Building on prior work (Reichl & Deike, 2020; Wanninkhof & Trinanes, 2017), the focus here is on global variability in temporal trends in k and F under high wind speed conditions (to be defined later). With improved knowledge of how winds affect long-term trends in global air-sea CO_2 exchange (Wanninkhof & Trinanes, 2017), the overarching question to be explored is how HW impact k and F globally when explicitly accounting for the bubble effect. The new k_{D18} is employed and contrasted with the widely used wind-only parameterization (Wanninkhof, 2014), labeled as k_{W14}. The manuscript is organized as follows: the datasets and data processing methods are introduced in Section 2. In Section 3, the climatological distribution and long-term trends in k along with concomitant F estimates are analyzed focusing on HW. Limitations and concluding remarks are presented in Section 4 and Section 5, respectively.

2. Materials and Methods

2.1. Parameterization of the Air-Sea CO_2 Flux

The coefficient of the wind-only formulation and gas transfer velocities depend on the wind product being used. The k_{W14}, as an update of a prior expression already in use in current climate models (Wanninkhof, 1992), is derived from the high-resolution Cross-Calibrated Multi-Platform (CCMP) wind product. This high-resolution wind product operating under short-term conditions is calibrated to match global ocean bomb-^{14}C inventories resulting in an "up-grade" to k_{W14} (Wanninkhof, 2014). The expression for k_{W14} is given as

$$k_{\mathrm{W14}} = aU^2\left(Sc\ /\ 660\right)^{-1/2} \tag{2}$$

where the coefficient "a" is 0.251 in the unit of (cm hr^{-1}) (m s^{-1})$^{-2}$. The Sc is the molecular Schmidt number (>>1) given by the ratio of the kinematic viscosity in seawater and the molecular diffusion coefficient of CO_2, U^2 is the squared wind speed (or twice the mean flow kinetic energy) measured at 10-m height.

The second expression employed here is a recently developed wind-wave dependent formulation (Deike & Melville, 2018). This formulation separates the bubble-mediated term k_b from the none-breaking term k_{nb} and results in a k_{D18} given as

$$k_{\mathrm{D18}} = k_{nb} + k_b = u_*\left[A_{NB}\left(\frac{S_c}{660}\right)^{-1/2} + \frac{A_B}{W_0}\left(\left(u_* {c_{wh}}^2\right)^{2/3}\right)\right] \tag{3}$$

where $A_{NB} = 1.55 \times 10^{-4}$, $A_B = 1 \pm 0.2 \times 10^{-5}$ m^{-2} s^2, W_0 is dimensionless Otswald solubility coefficient, $g = 9.8$ m s^{-2} is the gravitational acceleration, and H_s is the significant wave height, $c_{wh} = \sqrt{gH_s}$ is the ballistic speed, an important parameter for wave breaking, that can be related to the phase speed at the peak of the wave spectrum for fetch-limited conditions (Deike & Melville, 2018). The air-side friction velocity is $u_* = \left(\tau\ /\ \rho_{\mathrm{air}}\right)^{1/2}$, where ρ_{air} is the mean air density and τ is a turbulent shear stress assumed to be a function of U via the quadratic drag-law $\tau = \rho_{\mathrm{air}} C_D U^2$ with a wind-dependent drag coefficient C_D (at $z = 10$ m) derived elsewhere (Large, 2006). With this representation, u_* (m s^{-1}) can be related to an externally supplied U via

$$\frac{u_*}{U} = \sqrt{C_D} = \left[\left(\frac{A_{u1}}{U} + A_{u2} + A_{u3}U\right) \times 10^{-3}\right]^{1/2} \tag{4}$$

where $A_{u1} = 2.7$ (m s^{-1}), $A_{u2} = 0.142$ (dimensionless), and $A_{u3} = 0.076$ (s m^{-1}). This C_D representation allows k_{D18} to be expressed as a function of U, c_{wh}, and SST.

It is to be noted that the k_{W14} expression is based on matching long time integration fluxes (dual tracer technique) but using higher resolution U (6-hourly), while the data used to develop the k_{D18} formulation are fitted based on eddy covariance measurements of the flux in the atmosphere (with averaging intervals less than 15 min and sampling frequencies exceeding 10 Hz). Thus, the k_{D18} formulation has been calibrated and tested at a much higher temporal resolution. Reconciliation of estimates of k based on eddy covariance, dual tracer and other approaches is still debated in the community (Edson et al., 2011; Wanninkhof et al., 2009).

While the focus here is on HW, trends in k and F for all winds were also estimated. When including all wind conditions, the findings derived here parallel conclusions of Wanninkhof and Trinanes (2017), though different k formulations were used (see Figures S1 and S2).

2.2. Data Products

The U, H_s, SST, salinity, and pCO_2 data from 1990 to 2018 are used to compute global spatial patterns and trends in k and F at high U. All these data are linearly interpolated onto a spatial resolution of 0.5° and averaged to a daily temporal resolution. The 6-hourly CCMP-v2 wind speed data at the 0.25° grid are obtained from the Remote Sensing Systems described elsewhere (Atlas et al., 2011). This wind product is produced using satellite, moored buoy, and model wind data fusion, and it agrees with mooring records and other wind products described elsewhere (Kent et al., 2013; Wanninkhof & Trinanes, 2017). The CCMP product is available since 1987, but there are appreciable gaps in the records in 1988 and 1989. Therefore, the period from 1990 through 2018 is used here. Both 6-hourly SST and H_s data at 0.5°C resolution are derived from the European Centre for Medium-Range Weather Forecasts (ECMWF) fifth generation ERA5 reanalysis products described elsewhere (Copernicus Climate Change Service (C3S), 2017). ERA5 is the latest released climate dataset produced using ECMWF's Integrated Forecast System, which is coupled to an ocean wave model. A large fraction of H_s data are missing in polar regions due to ice coverage, especially in winter

(Figures S3 and S4). We thus set these missing values in H_s to zero (meaning no bubble contribution to k). The monthly climatological sea surface salinity data at 1° grid are obtained from World Ocean Atlas 2009 (WOA09) described elsewhere (Antonov et al., 2010).

The Sc for CO_2 is a function of SST and is determined using standard formulation (Wanninkhof & Trinanes, 2017). The solubility is expressed as a function of water temperature (T, in Kelvin) and salinity (S, in ‰) using the empirical relation (R. F. Weiss, 1974):

$$\ln\left(K_0\right) = A_1 + A_2\frac{100}{T} + A_2\ln\left(\frac{T}{100}\right) + S\left[B_1 + B_2\frac{T}{100} + B_3\left(\frac{T}{100}\right)^2\right] \tag{5}$$

where K_0 is the solubility (mol L^{-1} atm^{-1}). The numerical values for these coefficients are $A_1 = -58.0931$, $A_2 = 90.5069$, $A_3 = 22.2940$, $B_1 = -0.027766$, $B_2 = -0.025888$, and $B_3 = 0.0050578$. The dimensionless Otswald solubility coefficient W_0 is expressed as $W_0 = K_0RT$ (Keeling, 1993), where the ideal gas constant R is taken as 0.08205 L atm mol^{-1} k^{-1}.

The impact of U on trends in F was evaluated using averaged ΔpCO_2 estimates. The monthly climatological pCO_{2w} centered on year 2005 is from Takahashi et al. (2014). The pCO_{2a} for the 2005 reference year is calculated following the approach in Takahashi et al. (2009) and is given as

$$pCO_{2a} = xCO_{2a}\left(P_{baro} - P_{sw}\right) \tag{6}$$

where xCO_2 is the CO_2 mole fraction or mixing ratio, P_{baro} is the barometric pressure at the sea surface, P_{sw} is the water vapor pressure at seawater temperature. The xCO_2 data are retrieved from the NOAA greenhouse Gas Marine Boundary Layer Reference data product (Conway et al., 1994). The P_{baro} is from NCEP/NCAR Reanalysis 1 (Kalnay et al., 1996) and the P_{sw} is from NCAR/UCAR Atlas of Surface Marine Data.

2.3. External Factors Influencing *k* and *F*

A sensitivity analysis was conducted to evaluate the effects of changes in ΔpCO_2, U, SST, and H_s on k and F at high U by varying a given property while setting the other properties to their climatological means (Table S1). The starting values of ΔpCO_2 and salinity were set to −5.6 μatm and 34.74 psu, respectively according to climatological global mean salinity and the ΔpCO_2 in the reference year 2005. The starting values of U, SST, and H_s were set to 16.5 m s^{-1}, 8.5°C, and 4.8 m, respectively, according to their climatological global mean at high U.

Three scenarios of imposed changes are applied to estimate the sensitivity of k and F to factors listed in Table S1. Variations in SST, U, and H_s for the first two scenarios are based on temporal variability of globally averaged values at high U during the period 1990–2018. The third scenario is based on (climatological) spatial gradients between tropics and subpolar regions of these factors at high U, as discussed in Section 3.2. Imposed changes in ΔpCO_2 are in proportion to trends in differences in oceanic pCO_2 at Station ALOHA and atmospheric pCO_2 at Mauna Loa.

The sensitivity of k and F to each external factor was assessed from the ratio of the percentage change in k or F (labeled Y) to percentage change in each factor (labeled X) using

$$\text{Sensitivity} = \frac{\Delta Y\ /\ Y}{\Delta X\ /\ X} \tag{7}$$

3. Results and Discussion

We now define a HW as conditions for which $U > 15$m s^{-1}. This threshold is based on the rapid increase in bubble formation with increasing U. With the significant uptick in both frequency and magnitudes of HW over the last 3 decades (Figures 1a and 1b), we focus our efforts on the drivers of climatological and long-term trends in k and F at high U.

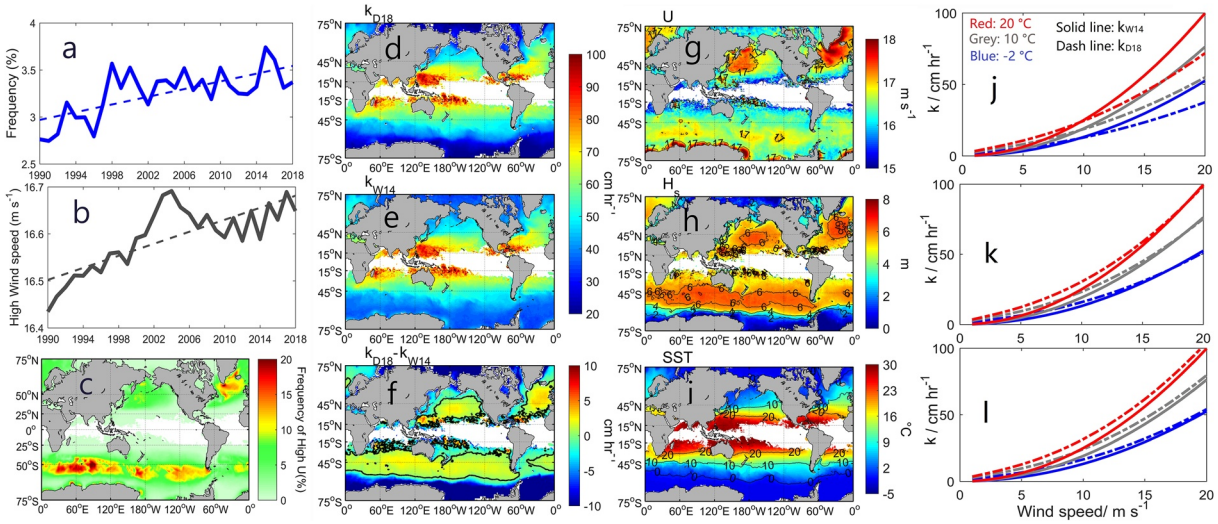

Figure 1. (a) Time series of global high winds ($U > 15$ m s^{-1}) frequency showing an increase in annual occurrences from 2.6% of the time to 3.3% over the last 3 decades. (b) Time series of the global average high wind ($U > 15$ m s^{-1}) also showing a concomitant increase in magnitude. (c) Map of the climatological mean frequency of high wind events (%). Maps of global climatological mean of (d) k_{D18}, (e) k_{W14}, (f) the difference (k_{D18}–k_{W14}), (g) wind speed (U), (h) significant wave height (H_s), and (i) Sea surface temperature (SST) at high U. The relations for k_{D18} (dashed curve), k_{W14} (solid curve), and U with different H_s: (j) 2 m, (k) 6 m, and (l) 7 m. SST of 20°C is in red, 10°C is in gray, and −2°C is in blue.

3.1. Spatial Pattern of Gas Transfer Velocity at High Winds

The global long-term averages of k at high U (k_{HW}) are approximately 49 cm hr^{-1} for k_{D18} and 51 cm hr^{-1} for k_{W14}, around 3–4 times higher than the overall mean k at all wind speeds. While HW are rare in tropical and subtropical regions (Figure 1c), they are associated with higher k than in subpolar and polar regions (Figures 1d and 1e). Interestingly, these extremes in k_{HW} are not associated with extreme winds (Figure 1g) or high waves (Figure 1h), but rather predominantly driven by warmer temperature (Figure 1i). The large geographical variability in SST (−2 to 30°C) and the narrow range of spatial variations in U (about 99% U in the range of 15–18 m s^{-1}) and H_s (5–7 m) at high U (Figure S5) explains the dominant role of SST in setting the spatial pattern of k_{HW} for both k parameterizations. As shown by the sensitivity analysis (Table S1), though the k_{HW} is much more sensitive to changes in U than SST and H_s, a 150% increase in SST (with a reference starting values of 8.5°C) from subpolar regions to tropical regions leads to a 20 cm hr^{-1} increase in k_{HW}. In contrast, changes in U and H_s (with references starting values of 16.5 m s^{-1} and 4.8 m, respectively) between subpolar regions and tropical regions could only induce up to 8 cm hr^{-1} changes in k_{HW}.

As expected, k_{D18} increases with H_s (Figures 1j–1l). The $k_{D18} > k_{W14}$ in regions experiencing frequent HW such as subtropical to subpolar regions (Figure 1f), likely results from H_s's contribution to the bubble parameterization in k_{D18} at high U (Figures 1h and 1l). In contrast, k_{D18} is generally smaller than k_{W14} at high U in polar regions (Figure 1f) where the average H_s is around 2 m (Figures 1h and 1j). Wind-only parameterization may therefore underestimate the bubble-enhanced exchange under high U and H_s conditions and overestimates bubble contributions in polar regions where H_s are lower than expected, potentially due to reduced wind fetch and wave-ice interaction near ice-covered regions, especially in winter (Ardhuin et al., 2020; Herman et al., 2019; Smith & Thomson, 2016; Squire, 2020; Voermans et al., 2019). However, uncertainties in bubble-mediated gas exchange velocities in polar and subpolar regions can have a significant impact on the net air-sea CO_2 exchange because intense ventilation and deep water formation occur in these regions.

Moreover, a comparison of k_{660} calculated using k_{D18} and k_{W14} to field measurements of k_{660} indeed suggest a better representation of gas exchange when explicitly accounting for the bubbles' contribution to gas exchange at high U (Figure S6).

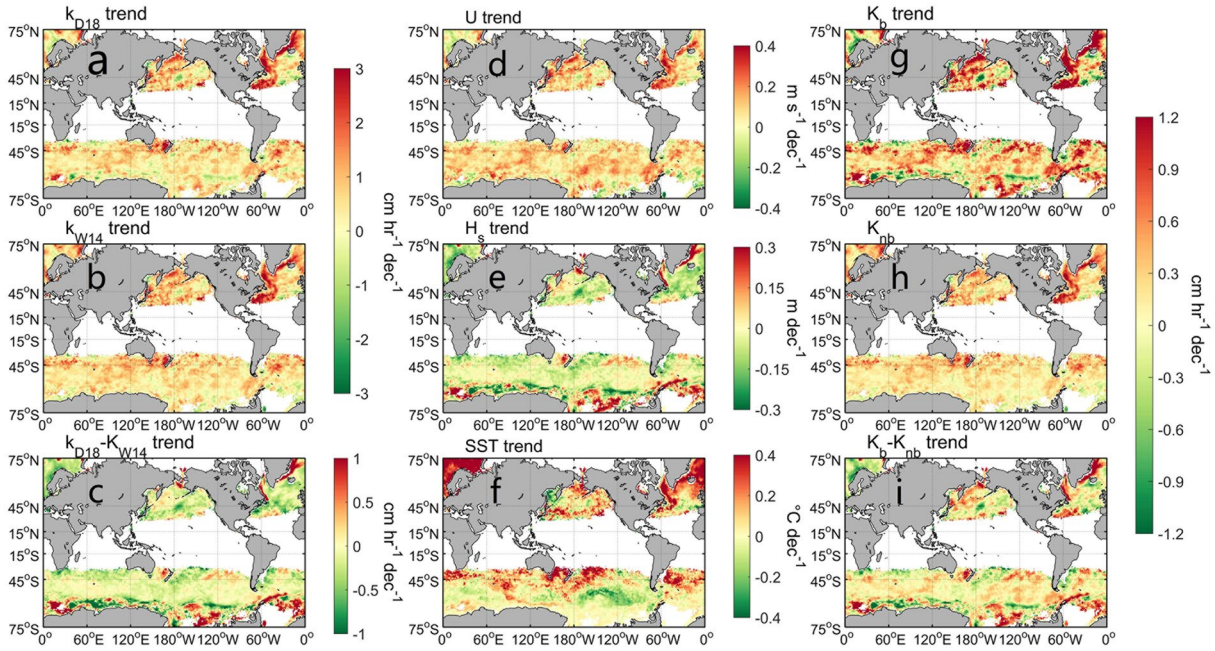

Figure 2. Maps of temporal trends in k and environmental factors at high U (>15 m s^{-1}) during the 1990–2018 period. Map of the long-term trend in (a) k_{D18}, (b) k_{W14}, (c) the difference (k_{D18}–k_{W14}), (d) wind speed (U), (e) significant wave height (H_s), (f) sea surface temperature (SST), (g) bubble term k_b, (h) non-bubble term k_{nb}, and (i) the difference (k_b–k_{nb}). Areas where HW does not occur every year are shown in blank. HW, high wind events.

3.2. Trends in Gas Transfer Velocity at High Winds

The global average k_{HW} is increasing at a rate of 0.7 cm hr^{-1} dec^{-1} over the last 3 decades (Figure S7). Spatially, the distribution of long-term trends in k_{HW} (Figures 2a and 2b) closely follows the trends in U at high U (U_{HW}; Figure 2d) with both generally increasing over time (and with no detectable saturation effect), consistent with trends in k_{HW} being dominantly driven by changes in U_{HW} over the global ocean. The global average SST at high U has been increasing faster than SST at all wind conditions (Figure S8). The trends in SSTs at high U (Figure 2f), such as in the North Atlantic, North Pacific, and regions along 45°S only marginally alter the trends in k_{HW}. As revealed by a sensitivity analysis conducted in the Northwest Atlantic, a 1.6% increase in U_{HW} (with a reference starting values of regional mean high U at 17.2 m s^{-1}) leads to an approximately 1.3 cm hr^{-1} increase in k_{HW}. In contrast, a 16% increase in SST (with references starting values of regional mean SST at high U at 1.9°C) could only lead to a 0.42 cm hr^{-1} increase in k_{HW}. While the global distribution of temporal trends in k_{D18} and k_{W14} agree, they differ in magnitude (Figure 2c), largely due to the impact of trend in H_s over the study period (Figure 2e, as expected from Equation 3).

To further evaluate the processes responsible for the long-term trends in k_{HW}, the bubble- and turbulence-mediated k_{HW} were analyzed independently. Spatially, the temporal trends in bubble-mediated air-sea gas flux kinetics (Figure 2g) appears to be controlled by U (or u_*) and less influenced by H_s (Figures 2d and 2e). A plausible explanation for these results is the sub-unity exponent for H_s and the above-unity exponent for u_* $\left(k_b \propto {u_*}^{5/3} {H_s}^{2/3}\right)$. In contrast, the spatial pattern of trends in non-bubble (turbulence) mediated gas flux kinetics at high U are predominantly determined by U (Figures 2h and 2d) because $k_{nb} \propto u_*$. The inconsistent trends in U and H_s observed here (Figures 2d and 2e) could be because the latter term is dominated by remotely generated swell rather than by local wind shear over large parts of the ocean (Semedo et al., 2011; Young, 1999; Young & Ribal, 2019). That U and H_s are not strongly coupled also allows exploring the sensitivity of k_{HW} to the aforementioned two variables to be treated separately.

For convenience, the ratio of bubble to turbulent contribution to k (= R_b) and thus the ratio of bubble component to overall flux as measured by R_{Fb} can be expressed as

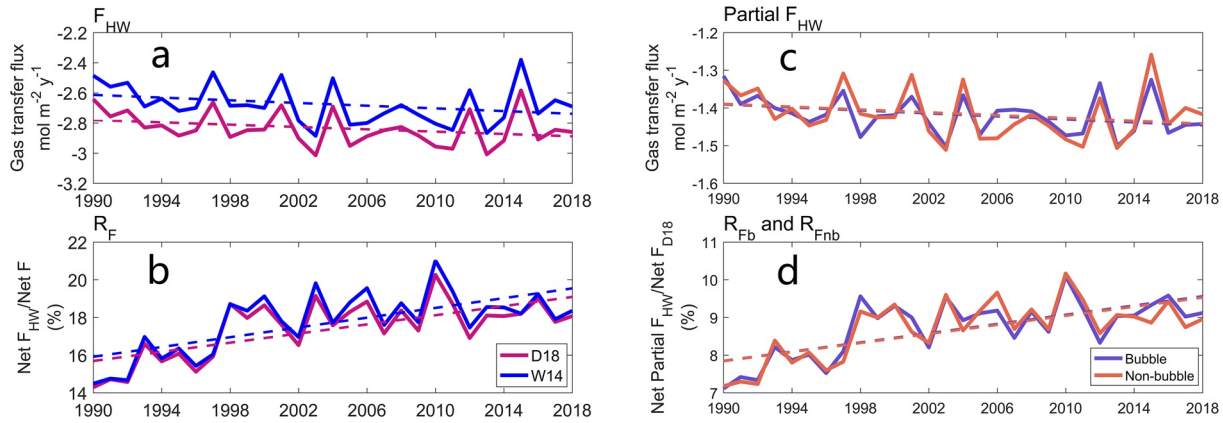

Figure 3. Temporal evolution of (a) spatially averaged flux at high U (F_{HW}), (b) the ratio (R_F) of net F at high U to global net F, (c) flux from the turbulent and bubble contributions at high U (Partial F_{HW}), (d) the ratio of bubble (R_{Fb}) and turbulent (R_{Fnb}) component under high winds to global net F quantified using k_{D18}. For (a) and (b), magenta represent F from k_{D18} (F_{D18}) and blue represent F from k_{W14} (F_{W14}). For (c) and (d), orange represent the turbulent component and purple represent the bubble component. The dashed line indicates the long-term trend. Negative signals mean CO_2 uptake by the ocean.

$$R_b = \frac{k_b}{k_{nb}} = \frac{A_B}{A_{NB}\, W_o}\left(\frac{S_c}{660}\right)^{1/2}\left(u_*\, {c_{wh}}^2\right)^{2/3}; R_{Fb} = \frac{F_b}{F} = \frac{R_b}{R_b + 1}, \tag{8}$$

where an $R_b >> 1$ results in an $R_{Fb} \approx 1$ and an $R_b = 1$ results in $R_{Fb} \approx 0.5$. As U increases, u_* and H_s increase, and c_{wh} generally also increases through H_s (because $c_{wh} = \sqrt{gH_s}$) thereby resulting in increased R_b with increased U. The estimate indicates that bubble contribution to k_{D18} is around 45% at high U conditions, which is expectedly greater than 30% estimated at all winds (Reichl & Deike, 2020; Woolf, 1997).

3.3. Trends in Air-Sea CO_2 Flux at High Winds

Interestingly, the most significant increases in k_{HW} is occurring in regions with high CO_2 exchange with the ocean interior through deep water formation and ventilation (Figure S9, e.g., the Southern Ocean and North Atlantic). As a result of these trends, we observe an enhancement in global mean CO_2 oceanic uptake at high U at rates of -0.040 mol m^{-2} y^{-1} dec^{-1} and -0.045 mol m^{-2} y^{-1} dec^{-1} when determined using k_{D18} and k_{W14}, respectively (Figure 3a; enhancement associated only with wind trends, keeping ΔpCO_2 constant). The ratio of net F at high U to the global net F measured by R_F is estimated and expressed as

$$R_F = \frac{\text{Net } F_{HW}}{\text{Net } F} = \frac{F_{HW}}{F}\frac{N_{HW}}{N} \tag{9}$$

where Net F_{HW} and Net F are in units of Pg C y^{-1}, F_{HW} and F are in units of mol m^{-2} y^{-1}, N is the number of the total oceanic grid, N_{HW} is the number of high wind grid (defined as a grid when daily U over 15 m s^{-1}). With a slightly negative trend in global mean F (Figure S2f), the contribution of HW to air-sea CO_2 exchange (R_F) increases as a result of increased magnitude (F_{HW}) and frequency (N_{HW}) at high U (with comparable trends for k_{D18} and k_{W14} expressions; Figure 3b and Equation 9). As shown by Equation 8, with increasing contribution from bubbles (i.e., R_b), the bubble-associated flux contribution to total CO_2 flux (R_{Fb}) increases as a saturation function at high U (Figure 3d). Globally, we estimate R_{Fb} at about 36%, which is commensurate with earlier estimates of some 40% (Reichl & Deike, 2020). However, at high U, R_{Fb} reaches as high as 50% (i.e., $R_b = 1$). These results suggest that both turbulent and bubble contributions have comparable effects on F at high U and both components should be considered in future climate studies. Overall, trends in HW are significant because, despite representing a minor fraction of total winds (3%), they disproportionately contribute to air-sea CO_2 exchange (18%).

4. Caveats and Limitations

Our study carries limitations that warrant further elaboration. First, the k_{D18} and k_{W14} expressions do not explicitly consider bubble-induced supersaturation. Using Large Eddy Simulations coupled with bubble dynamics and a transport model, Liang et al. (2020) showed that bubble supersaturation under hurricane conditions can substantially suppress CO_2 outgassing. It is difficult to extrapolate their results here as hurricane winds commence at 33 m/s, while 99% of the HW considered here are in the range of 15–18 m/s (Figure S5a). Furthermore, the gas transfer velocities estimated using k_{D18} are in good agreement with eddy covariance field measurements for U in the range of 0–25 m/s. Hence, the k_{D18} may indirectly include bubble-induced supersaturation effect though it remains unclear whether the equation derived in CO_2 sink regions can be applied in CO_2 source regions (Liang et al., 2020). Second, time-averaged U products can introduce some biases in all k due to the non-linear relation between U and k (Wanninkhof, 2002), a topic that is better kept for a future inquiry. Third, the C_D expression linking friction velocity to U required by k_{D18} does not consider thermal stratification in the atmosphere. However, the focus here is on high U where mechanical production of turbulent kinetic energy far exceeds buoyancy forces. Finally, the results may be dependent on the particular ΔpCO_2 product employed to estimate F. To ascertain that the overall results are independent of the ΔpCO_2 product, we re-ran the analyses with the ΔpCO_2 data of Landschützer et al. (2014). While the gas transfer velocities are independent of the ΔpCO_2 product, the contribution of HW to CO_2 fluxes differs in the precise magnitude but not the trends. For the two ΔpCO_2 products employed, HW events become increasingly significant over time in air-sea CO_2 fluxes (Figure S10).

5. Conclusions

Wind speed observations covering the 1990–2018 period and recent gas exchange parameterizations were used to examine the importance of synoptic high-wind events on CO_2 fluxes. These HW are linked to situations when bubbles are expected to play a significant role in gas transfer velocity and air-sea CO_2 gas exchange. Given the large spatial variations in SST, it is the primary variable explaining the time-averaged spatial variability in k when conditioned on high wind speeds only (i.e., k_{HW} for both parameterizations). This finding is in contrast to the distribution of k for all winds condition, which is primarily driven by wide variations in U (Figure S11). With increasing occurrence and magnitude of high winds, the intensifying k_{HW} increases air-sea CO_2 exchange. It is shown here that approximately 50% of the global CO_2 flux is attributed to the bubble-mediated exchange at high wind speeds. Hotspots of natural and anthropogenic CO_2 exchange and transfer to the ocean interior occur in high wind regions, such as the North Atlantic and the Southern Ocean. With current and projected increases in both intensity and frequency of extreme wind events (Young & Ribal, 2019; Young et al., 2011; Zheng et al., 2016), it is becoming necessary to quantify such fine-scaled processes that have disproportionate impact on air-sea CO_2 fluxes.

Data Availability Statement

The cross-calibrated multi-platform (CCMP-V2) 6-hourly wind speed are publicly available at www.remss.com/measurements/ccmp. The climatological pCO_{2w} data centered on 2005 was obtained from https://www.ldeo.columbia.edu/res/pi/CO2/carbondioxide/global_ph_data/obsfile.txt. The significant wave height and sea surface temperature data were obtained from https://cds.climate.copernicus.eu/cdsapp#!/dataset/reanalysis-era5-single-levels?tab=overview.

Acknowledgments
Y. Gu is supported by scholarship from China Scholarship Council (CSC) under the grant CSC 201906710071. G. Katul acknowledges support from the U.S. National Science Foundation (NSF-AGS-1644382, NSF-AGS-2028633, and NSF-IOS-1754893). N. Cassar is supported by the "Laboratoire d'Excellence" LabexMER (ANR-10-LABX-19) and cofunded by a grant from the French government under the program "Investissements d'Avenir." W. Zhang is supported in part by the scholarship from China Scholarship Council (CSC) under grant CSC 201806710104

References

Antonov, J. I., Seidov, D., Boyer, T. P., Locarnini, R. A., Mishonov, A. V., Garcia, H. E., et al. (2010). World Ocean Atlas 2009, Volume 2: Salinity. In S. Levitus (Ed.), *NOAA Atlas NESDIS* (Vol. *69*, p. 184). Washington, DC: U.S. Government Printing Office.

Ardhuin, F., Otero, M., Merrifield, S., Grouazel, A., & Terrill, E. (2020). Ice breakup controls dissipation of wind waves across Southern Ocean sea ice. *Geophysical Research Letters*, *47*(13), e2020GL087699. https://doi.org/10.1029/2020GL087699

Atlas, R., Hoffman, R. N., Ardizzone, J., Leidner, S. M., Jusem, J. C., Smith, D. K., & Gombos, D. (2011). A cross-calibrated, multiplatform ocean surface wind velocity product for meteorological and oceanographic applications. *Bulletin of the American Meteorological Society*, *92*(2), 157–174. https://doi.org/10.1002/2017JC013181

Bates, N. R. (2007). Interannual variability of the oceanic CO_2 sink in the subtropical gyre of the North Atlantic Ocean over the last 2 decades. *Journal of Geophysical Research*, *112*, C09013. https://doi.org/10.1029/2006JC003759

Bates, N. R., Knap, A. H., & Michaels, A. F. (1998). Contribution of hurricanes to local and global estimates of air-sea exchange of CO_2. *Nature*, *395*(6697), 58–61. https://doi.org/10.1038/25703

Bell, T. G., Landwehr, S., Miller, S. D., De Bruyn, W. J., Callaghan, A. H., Scanlon, B., & Saltzman, E. S. (2017). Estimation of bubble-mediated air-sea gas exchange from concurrent DMS and CO_2 transfer velocities at intermediate-high wind speeds. *Atmospheric Chemistry and Physics*, *17*(14), 9019–9033. https://doi.org/10.5194/acp-17-9019-2017

Blomquist, B. W., Brumer, S. E., Fairall, C. W., Huebert, B. J., Zappa, C. J., Brooks, I. M., & Czerski, H. (2017). Wind speed and sea state dependencies of air-sea gas transfer: Results from the high wind speed gas exchange study (HiWinGS). *Journal of Geophysical Research: Oceans*, *122*(10), 8034–8062. https://doi.org/10.1002/2017JC013181

Broecker, H. C., Petermann, J., & Siems, W. (1978). The influence of wind on CO_2-exchange in a wind-wave tunnel, including the effects of monolayers. *Journal of Marine Research*, *36*(4), 595–610.

Chelton, D. B., Schlax, M. G., Freilich, M. H., & Milliff, R. F. (2004). Satellite measurements reveal persistent small-scale features in ocean winds. *Science*, *303*(5660), 978–983. https://doi.org/10.1126/science.1091901

Conway, T. J., Tans, P. P., Waterman, L. S., Thoning, K. W., Kitzis, D. R., Masarie, K. A., & Zhang, N. (1994). Evidence for interannual variability of the carbon cycle from the NOAA/CMDL global air sampling network. *Journal of Geophysical Research*, *99*(22), 22831–22855. https://doi.org/10.1029/94JD01951

Copernicus Climate Change Service (C3S). (2017). *ERA5: Fifth generation of ECMWF atmospheric reanalyzes of the global climate Copernicus Climate Change Service Climate Data Store (CDS)*.

Deike, L., & Melville, W. K. (2018). Gas transfer by breaking waves. *Geophysical Research Letters*, *45*(19), 10482. https://doi.org/10.1029/2018GL078758

Edson, J. B., Fairall, C. W., Bariteau, L., Zappa, C. J., Cifuentes-Lorenzen, A., McGillis, W. R., et al. (2011). Direct covariance measurement of CO_2 gas transfer velocity during the 2008 Southern Ocean Gas Exchange Experiment: Wind speed dependency. *Journal of Geophysical Research*, *116*(C4). https://doi.org/10.1029/2011JC007022

Frew, N. M., Bock, E. J., Schimpf, U., Hara, T., Haußecker, H., Edson, J. B., & Jähne, B. (2004). Air-sea gas transfer: Its dependence on wind stress, small-scale roughness, and surface films. *Journal of Geophysical Research*, *109*(C8). https://doi.org/10.1029/2003JC002131

Herman, A., Cheng, S., & Shen, H. H. (2019). Wave energy attenuation in fields of colliding ice floes – Part 1: Discrete-element modeling of dissipation due to ice-water drag. *The Cryosphere*, *13*(11). https://doi.org/10.5194/tc-13-2887-2019

Ho, D. T., Bliven, L. F., Wanninkhof, R. I. K., & Schlosser, P. (1997). The effect of rain on air-water gas exchange. *Tellus B: Chemical and Physical Meteorology*, *49*(2), 149–158. https://doi.org/10.3402/tellusb.v49i2.15957

Huang, P., & Imberger, J. (2010). Variation of pCO_2 in ocean surface water in response to the passage of a hurricane. *Journal of Geophysical Research*, *115*, C10024. https://doi.org/10.1029/2010JC006185

Johnson, M. T., & Liss, P. S. (2014). *Ocean-atmosphere interactions of gases and particles* (p. 315). New York, NY: Springer Nature. https://doi.org/10.1007/978-3-642-25643-1_4

Kalnay, E., Kanamitsu, M., Kistler, R., Collins, W., Deaven, D., Gandin, L., & Zhu, Y. (1996). The NCEP/NCAR 40-year reanalysis project. *Bulletin of the American Meteorological Society*, *77*(3), 437–472.

Keeling, R. F. (1993). On the role of large bubbles in air-sea gas exchange and supersaturation in the ocean. *Journal of Marine Research*, *51*(2), 237–271. https://doi.org/10.1357/0022240933223800

Kent, E. C., Fangohr, S., & Berry, D. I. (2013). A comparative assessment of monthly mean wind speed products over the global ocean. *International Journal of Climatology*, *33*(11), 2520–2541. https://doi.org/10.1002/joc.3606

Landschützer, P., Gruber, N., Bakker, D. C. E., & Schuster, U. (2014). Recent variability of the global ocean carbon sink. *Global Biogeochemical Cycles*, *28*, 927–949. https://doi.org/10.1002/2014gb004853

Large, W. B. (2006). Surface fluxes for practitioners of global ocean data assimilation. In *Ocean weather forecasting* (pp. 229–270). Dordrecht: Springer.

Le Quéré, C., Takahashi, T., Buitenhuis, E. T., Rödenbeck, C., & Sutherland, S. C. (2010). Impact of climate change and variability on the global oceanic sink of CO_2. *Global Biogeochemical Cycles*, *24*(4). https://doi.org/10.1029/2009GB003599

Lévy, M., Lengaigne, M., Bopp, L., Vincent, E. M., Madec, G., Ethé, C., et al. (2012). Contribution of tropical cyclones to the air-sea CO_2 flux: A global view. *Global Biogeochemical Cycles*, *26*, GB2001. https://doi.org/10.1029/2011GB004145

Liang, J.-H., D'Asaro, E. A., McNeil, C. L., Fan, Y., Harcourt, R. R., Emerson, S. R., et al. (2020). Suppression of CO_2 outgassing by gas bubbles under a hurricane. *Geophysical Research Letters*, *47*, e2020GL090249. https://doi.org/10.1029/2020GL090249

Liss, P. S., & Merlivat, L. (1986). Air-sea gas exchange rates: Introduction and synthesis. In *The role of air-sea exchange in geochemical cycling* (pp. 113–127). Dordrecht: Springer.

McGillis, W. R., Edson, J. B., Ware, J. D., Dacey, J. W., Hare, J. E., Fairall, C. W., & Wanninkhof, R. (2001). Carbon dioxide flux techniques performed during GasEx-98. *Marine Chemistry*, *75*(4), 267–280. https://doi.org/10.1016/s0304-4203(01)00042-1s

Minobe, S., Kuwano-Yoshida, A., Komori, N., Xie, S. P., & Small, R. J. (2008). Influence of the Gulf stream on the troposphere. *Nature*, *452*(7184), 206–209. https://doi.org/10.1038/nature06690

Nightingale, P., Malin, G., Law, C. S., Watson, A. J., Liss, P. S., Liddicoat, M. I., et al. (2000). In situ evaluation of air-sea gas exchange parameterizations using novel conservative and volatile tracers. *Global Biogeochemical Cycles*, *14*(1), 373–387. https://doi.org/10.1029/1999GB900091

Prytherch, J., Yelland, M. J., Pascal, R. W., Moat, B. I., Skjelvan, I., & Srokosz, M. A. (2010). Open ocean gas transfer velocity derived from long-term direct measurements of the CO_2 flux. *Geophysical Research Letters*, *37*(23). https://doi.org/10.1029/2010GL045597

Reichl, B. G., & Deike, L. (2020). Contribution of sea-state dependent bubbles to air-sea carbon dioxide fluxes. *Geophysical Research Letters*, *47*, e2020GL087267. https://doi.org/10.1029/2020GL087267

Sampe, T., & Xie, S. P. (2007). Mapping high sea winds from space: A global climatology. *Bulletin of the American Meteorological Society*, *88*(12), 1965–1978. https://doi.org/10.1175/BAMS-88-12-1965

Semedo, A., Sušelj, K., Rutgersson, A., & Sterl, A. (2011). A global view on the wind sea and swell climate and variability from ERA-40. *Journal of Climate*, *24*(5), 1461–1479. https://doi.org/10.1175/2010JCLI3718.1

Small, R. D., deSzoeke, S. P., Xie, S. P., O'neill, L., Seo, H., Song, Q., & Minobe, S. (2008). Air–sea interaction over ocean fronts and eddies. *Dynamics of Atmospheres and Oceans*, *45*(3–4), 274–319. https://doi.org/10.1016/j.dynatmoce.2008.01.001

Smith, M., & Thomson, J. (2016). Scaling observations of surface waves in the Beaufort Sea. *Elementa Science of the Anthropocene*, *4*(97), 1–12. https://doi.org/10.12952/journal.elementa.000097

Spall, M. A. (2007). Midlatitude wind stress-sea surface temperature coupling in the vicinity of oceanic fronts. *Journal of Climate*, *20*(15), 3785–3801. https://doi.org/10.1175/JCLI4234.1

Squire, V. A. (2020). Ocean wave interactions with sea ice: A reappraisal. *Annual Review of Fluid Mechanics*, *52*, 37–60. https://doi.org/10.1146/annurev-fluid-010719-060301

Sweeney, C., Gloor, E., Jacobson, A. R., Key, R. M., McKinley, G., Sarmiento, J. L., & Wanninkhof, R. (2007). Constraining global air-sea gas exchange for CO_2 with recent bomb ^{14}C measurements. *Global Biogeochemical Cycles*, *21*(2). https://doi.org/10.1029/2006GB002784

Takahashi, T., Sutherland, S. C., Chipman, D. W., Goddard, J. C., Ho, C., Newberger, T., et al. (2014). Climatological distributions of pH, pCO_2, total CO_2, alkalinity, and $CaCO_3$ saturation in the global surface ocean, and temporal changes at selected locations. *Marine Chemistry*, *164*, 95–125. https://doi.org/10.1016/j.marchem.2014.06.004

Takahashi, T., Sutherland, S. C., Wanninkhof, R., Sweeney, C., Feely, R. A., Chipman, D. W., & Watson, A. (2009). Climatological mean and decadal change in surface ocean pCO_2, and net sea-air CO_2 flux over the global oceans. *Deep Sea Research Part II: Topical Studies in Oceanography*, *56*(8–10), 554–577. https://doi.org/10.1016/j.dsr2.2008.12.009

Voermans, J. J., Babanin, A. V., Thomson, J., Smith, M. M., & Shen, H. H. (2019). Wave attenuation by sea ice turbulence. *Geophysical Research Letters*, *46*(12), 6796–6803. https://doi.org/10.1029/2019GL082945

Wanninkhof, R. (1992). Relationship between wind speed and gas exchange over the ocean. *Journal of Geophysical Research*, *97*(C5), 7373–7382. https://doi.org/10.1029/92JC00188

Wanninkhof, R. (2014). Relationship between wind speed and gas exchange over the ocean revisited. *Limnology and Oceanography: Methods*, *12*(6), 351–362. https://doi.org/10.4319/lom.2014.12.351

Wanninkhof, R., Asher, W. E., Ho, D. T., Sweeney, C. S., & McGillis, W. R. (2009). Advances in quantifying air-sea gas exchange and environmental forcing. *Annual Review of Marine Science*, *1*, 213–244. https://doi.org/10.1146/annurev.marine.010908.163742

Wanninkhof, R., & McGillis, W. R. (1999). A cubic relationship between air-sea CO_2 exchange and wind speed. *Geophysical Research Letters*, *26*(13), 1889–1892. https://doi.org/10.1029/1999GL900363

Wanninkhof, R., & Trinanes, J. (2017). The impact of changing wind speeds on gas transfer and its effect on global air-sea CO_2 fluxes. *Global Biogeochemical Cycles*, *31*(6), 961–974. https://doi.org/10.1002/2016GB005592

Watson, A. J., Schuster, U., Shutler, J. D., Holding, T., Ashton, I. G., Landschützer, P., & Goddijn-Murphy, L. (2020). Revised estimates of ocean-atmosphere CO_2 flux are consistent with ocean carbon inventory. *Nature Communications*, *11*(1), 1–6. https://doi.org/10.1038/s41467-020-1820

Weiss, A., Kuss, J., Peters, G., & Schneider, B. (2007). Evaluating transfer velocity-wind speed relationship using a long-term series of direct eddy correlation CO_2 flux measurements. *Journal of Marine Systems*, *66*(1–4), 130–139. https://doi.org/10.1016/j.jmarsys.2006.04.011

Weiss, R. F. (1974). Carbon dioxide in water and seawater: The solubility of a non-ideal gas. *Marine Chemistry*, *2*(3), 203–215. https://doi.org/10.1016/0304-4203(74)90015-2

Woolf, D. K. (1993). Bubbles and the air-sea transfer velocity of gases. *Atmosphere-Ocean*, *31*(4), 517–540. https://doi.org/10.1029/2018GB006041

Woolf, D. K. (1997). Bubbles and their role in gas exchange. In *The sea surface and global change* (pp. 173–206). Cambridge: Cambridge University Press. https://doi.org/10.1017/CBO9780511525025.007

Xie, S. P. (2004). Satellite observations of cool ocean-atmosphere interaction. *Bulletin of the American Meteorological Society*, *85*(2), 195–208. https://doi.org/10.1175/BAMS-85-2-195

Young, I. R. (1999). Seasonal variability of the global ocean wind and wave climate. *International Journal of Climatology: A Journal of the Royal Meteorological Society*, *19*(9), 931–950. https://doi.org/10.1002/(SICI)1097-0088(199907)19:9<931::AID-JOC412>3.0.CO;2-O

Young, I. R., & Ribal, A. (2019). Multiplatform evaluation of global trends in wind speed and wave height. *Science*, *364*(6440), 548–552. https://doi.org/10.1126/science.aav9527

Young, I. R., Zieger, S., & Babanin, A. V. (2011). Global trends in wind speed and wave height. *Science*, *332*(6028), 451–455. https://doi.org/10.1126/science.1197219

Zappa, C. J., McGillis, W. R., Raymond, P. A., Edson, J. B., Hintsa, E. J., Zemmelink, H. J., et al. (2007). Environmental turbulent mixing controls on air-water gas exchange in marine and aquatic systems. *Geophysical Research Letters*, *34*(10). https://doi.org/10.1029/2006GL028790

Zheng, C. W., Pan, J., & Li, C. Y. (2016). Global oceanic wind speed trends. *Ocean & Coastal Management*, *129*, 15–24. https://doi.org/10.1016/j.ocecoaman.2016.05.001